Korean J. Chem. Eng., **31**(4), 712-718 (2014)
DOI: 10.1007/s11814-013-0289-z

pISSN: 0256-1115
eISSN: 1975-7220

Supercapacitive behavior of mesoporous carbon CMK-3 in calcium nitrate aqueous electrolyte

Heming Luo*, Liwen Zheng*, Longyan Lei*, Deyi Zhang*,,***,†, Jingxiang Wu*, and Jian Yang***

*College of Petrochemical Technology, Lanzhou University of Technology, Lanzhou 730050, China
**State Key Laboratory of Gansu Advanced Non-ferrous Metal Materials,
Lanzhou University of Technology, Lanzhou 730050, China
***Key Laboratory of Eco-Environment-Related Polymer Materials of the Ministry of Education,
Northwest Normal University, Lanzhou 730070, China
(*Received 5 June 2013 • accepted 23 December 2013*)

Abstract−Calcium nitrate $Ca(NO_3)_2$ aqueous solution was found to be an effective aqueous electrolyte for a supercapacitor using ordered mesoporous carbon as the electrode materials. The supercapacitive behavior of ordered mesoporous carbon CMK-3 electrode in $Ca(NO_3)_2$ aqueous electrolyte was investigated utilizing cyclic voltammetry (CV), electrochemical impedance spectroscopy (EIS), and galvanostatic charge/discharge measurements. CMK-3 electrode shows excellent supercapacitive behavior with wide voltage window, high specific gravimetric capacitance and satisfactory electrochemical stability in $Ca(NO_3)_2$ aqueous electrolyte. The specific gravimetric capacitance of CMK-3 electrode in $Ca(NO_3)_2$ aqueous electrolyte reaches 210 F g^{-1} at a current density of 1 A g^{-1}, which is higher than that in conventional aqueous electrolytes $NaNO_3$ and KOH solution about 40% and 54%, respectively. The high charge density of the electric double layer formed at the interface of the CMK-3 electrode and $Ca(NO_3)_2$ aqueous electrolyte and the pseudo-capacitive effect originating from the oxygen groups on the surface of CMK-3 were believed to respond for the excellent supercapacitive behavior of CMK-3 electrode in $Ca(NO_3)_2$ aqueous electrolyte.

Keywords: Mesoporous Carbon, $Ca(NO_3)_2$, Aqueous Electrolytes, Supercapacitive Behavior

INTRODUCTION

Supercapacitors, a new type of energy storage device, have recently received much attention owing to their considerable capacitance, large power density, moderate energy density, and longer cycle-life [1-4]. The electrochemical supercapacitor utilizes the electrochemical double layer formed at the interface of the electrode and electrolyte or the pseudo-capacitance originates from the faradaic interactions between the ions of electrolytes and the solid electrode surface to store electric charge [5,6]. Thus, the electrolyte is believed as one of the key factors determining the performance of the supercapacitor. In general, aqueous electrolytes can provide high energy and power densities and be compatible with the supercapacitor industry [7]. At the present, most of the research on aqueous electrolytes is focused on the univalent cation aqueous, such as KOH [2,8], H_2SO_4 [9,10] and $NaNO_3$ [11] aqueous solution. Recently, polyvalent cation aqueous electrolyte, such as $Ca(NO_3)_2$, was found to be more efficient than univalent cation for supercapacitor based on manganese oxides electrode materials, which stores the electrical energy in the form of pseudo-capacitance [12]. The enhanced pseudo-capacitance of MnO_2 in polyvalent cations is believed to be originate from the adsorption-desorption of cations (M^{n+}) on the oxide surface [12]:

$$(MnO_2)_{surface}+M^{n+}+ne\rightarrow(MnO_2^{n-}\ M^{n+})_{surface}$$

Carbon materials with high surface areas, such as activated carbons, ordered mesoporous carbon, carbon nanotubes and graphene, are another type of common electrode material for supercapacitor, which stores the electrical energy mainly in the form of electrochemical double layer capacitance [1,13]. The effects of the polyvalent cation aqueous electrolytes on the supercapacitive behavior of these electrode materials are rarely reported. From the fundamental point of view, the polyvalent cations are more advantageous than univalent cations because of the fact that each polyvalent cation adsorbed onto the surface of electrode material would provide two or even three electrons for electric double layer, which is favorable for the electrostatic attraction between the electrode and electrolyte. This would enhance the charge density of the electric double layer, and then reasonably enhance the capacitive performance of the supercapacitor. Therefore, if this mechanism is possible, it seems that the capacitance of carbon materials could be improved only through the usage of polyvalent cations in place of traditional univalent cations.

We investigated the supercapacitive behavior of the common carbon electrode materials, ordered mesoporous carbon CMK-3, in $Ca(NO_3)_2$ aqueous electrolyte and compared with that in univalent cation aqueous electrolytes KOH and $NaNO_3$ to identify the effects of polyvalent cation on the capacitive performance of supercapacitor.

EXPERIMENTAL

1. Synthesis of Ordered Mesoporous Carbon CMK-3

The mesoporous silica template SBA-15 was synthesized using triblock copolymer Pluronic P123 as a template and tetraethoxytitane (TEOS) as a silica source [14]. The ordered mesoporous carbons CMK-3 was synthesized according to the reported procedures [15].

†To whom correspondence should be addressed.
E-mail: lzdeyizhang@gmail.com, lzdeyizhang@yahoo.cn

In a typical synthesis, 1 g of SBA-15 template was mixed with an aqueous solution consisting of 1.25 g of sucrose, 0.14 g of H_2SO_4, and 5.0 g of H_2O. The resultant viscous mixture was placed in a drying oven for 6 h at 373 K, and subsequently the oven temperature was increased to 433 K and maintained at the same temperature for 6 h. The sample turned dark brown during the treatment in the oven. After heating, the silica powder containing partially decomposed sucrose was mixed with aqueous solution consisting of 0.75 g of sucrose, 0.09 g of H_2SO_4, and 5.0 g of H_2O. After heating at 433 K again, the sucrose solution gradually dried, connecting the powder as a monolith. The carbonization of the monolith was completed by pyrolysis with heating to 1,073 K under a nitrogen atmosphere for 4 h. Finally, the silica template was removed by dissolving in HF aqueous solution (10 wt%) to obtain CMK-3.

2. Materials Characterization

X-ray diffraction patterns (XRD) were collected on an X'Pert X-ray defractometer (Phillips) using Cu Kα radiation. The d spacing values were calculated by the formula $d=\lambda/2\sin\theta$, and the unit cell parameters were calculated from the formula $a=2\times3^{-1/2}d_{100}$. The wall thickness was calculated from $W_T=a-D$, where a represents the unit cell parameter and D is the pore diameter calculated from the N_2 sorption measurements. Nitrogen adsorption/desorption isotherms were measured at 77 K with a Micromeritics ASAP 2020 volumetric adsorption analyzer. Prior to each adsorption measurement the samples were evacuated at 100 °C under vacuum ($p<10^{-5}$ mbar) in the degas port. The specific surface area, S_{BET} was determined from the linear part of the Brunauer, Emmett and Teller (BET) equation. The pore volume was calculated using the BET plot from the amount of nitrogen gas adsorbed at the last adsorption point ($P/P_0=0.95$), and the pore size distribution using the Barrett-Joyner-Halenda (BJH) method. Transmission electron microscopy (TEM) experiments were conducted on a JEM-2010 microscope operated at 200 kV. The samples for TEM measurements were suspended in ethanol and dried on a holey carbon film on a Cu grid. X-ray photoelectron spectroscopy (XPS) was performed on a Thermo Multilab 2000, using Monochrome Al Kα as the excitation source. Fourier transform infrared (FTIR) spectra were carried out on a Nicolet IS5 spectrometer using KBr pallets at ambient temperature.

3. Electrochemical Measurements

The electrochemical measurements, including cyclic voltammetry (CV), galvanostatic charge/discharge measurements, and electrochemical impedance spectroscopy (EIS), were performed with an electrochemical analyzer, CHI 660D (Shanghai, Chenhua Limited Co.) under ambient conditions in $Ca(NO_3)_2$ (2 M), KOH (2 M) and $NaNO_3$ (2 M) aqueous solution respectively, using a three-electrode system, with CMK-3 as the working electrode, a platinum slice as the counter electrode and an SCE (saturated calomel electrode) as the reference electrode. To prepare the working electrode, CMK-3 was ground with acetylene black (10 wt%) and polytetrafluoroethylene (PTFE, 5 wt%), and then pressed onto nickel foam that served as a current collector.

The specific gravimetric capacitance (C_g) for the CMK-3 in dif-

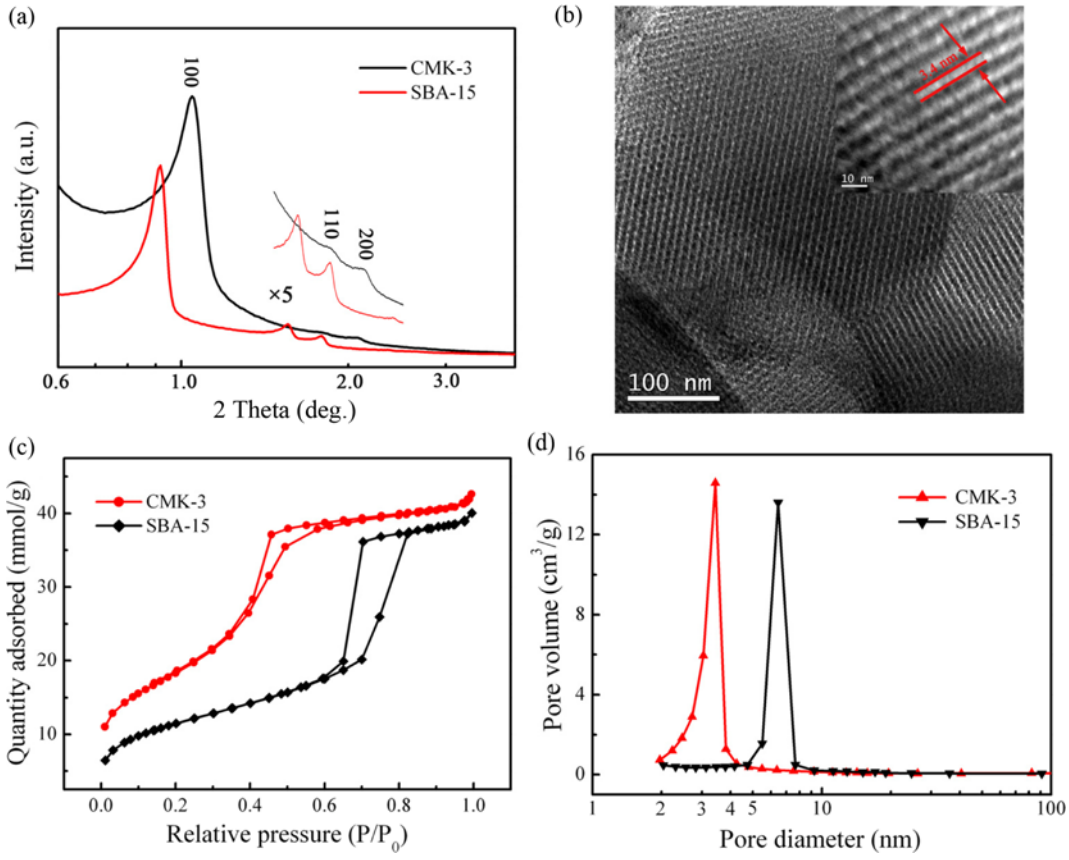

Fig. 1. SAXS patterns of CMK-3 and SBA-15 (a); TEM images of CMK-3 (b); N_2 adsorption-desorption isotherms of CMK-3 and SAB-15 (c); pore size distribution of CMK-3 and SBA-15 (d).

Table 1. Textural parameters of CMK-3 and SBA-15 template

Samples	d_{100} [nm]	a [nm]	D [nm]	W_T [nm]	S_{BET} [$m^2 g^{-1}$]	V_T [$cm^3 g^{-1}$]	V_M [$cm^3 g^{-1}$]
SBA-15	9.5	10.97	6.58	4.39	930	1.44	1.34
CMK-3	8.3	9.58	3.43	6.06	1480	1.59	1.43

ferent aqueous electrolyte is obtained from the charge-discharge curves and it can be calculated as:

$$C_g = \frac{I \times t}{\Delta V \times m} \quad (1)$$

where I is the discharge current, m the mass of the corresponding electrode materials, t the discharge time, and ΔV is the voltage range.

RESULTS AND DISCUSSIONS

1. Structure and Textural Properties of CMK-3

CMK-3 successfully replicated the mesostructure of SBA-15 template. As shown in Fig. 1(a), the SAXS patterns for CMK-3 exhibit three well-resolved diffraction peaks, associated with 100, 110, and 200 reflections of 2D hexagonal symmetry with the space group of *p6mm* [16]. Framework shrinkage during the pyrogenation/carbonization process of the precursor can be observed, as shown in Table 1; the cell parameter (a) is calculated to be 9.58 nm for CMK-3, which is lower than that of SBA-15 template (10.97 nm). The shift of diffraction peaks to higher angle provides directly evidence for this shrinkage phenomenon [4]. TEM images of the CMK-3 (Fig. 4(b)) clearly display uniform stripe-like and hexagonally arranged images. The wall thickness estimated from the TEM images is ca. 6 nm, which is very close to the pore diameter of SBA-15 template (6.58 nm). This clearly demonstrates that ordered mesoporous carbon CMK-3 with 2D hexagonal (*p6mm*) mesostructure has been truly replicated from the SBA-15 mesoporous silica template.

The nitrogen adsorption/desorption isotherms and pore size distribution of the CMK-3 and SBA-15 template are shown in Fig. 1(c) and (d), respectively. The textural parameters of the corresponding samples are listed in Table 1. As shown in Fig. 1(c), the isotherms of CMK-3 exhibit type IV adsorption behavior with an H1 hysteresis loop at higher relative pressure, ranging from 0.4 to 0.9 in the adsorption isotherms. The sharp steps corresponding to the capillary condensation of nitrogen inside the ultra-large mesopores reveal the narrow pore size distribution of the mesoporous carbon materials. The step of adsorption branch shifts to the lower relative pressure compared with that of SBA-15 template, implying a decrement of pore size. The pore size distribution curves of the CMK-3 sample (Fig. 1(d)) exhibit a sharp peak at 3.43 nm, indicating that CMK-3 has a uniform pore structure. Owing to the framework shrinkage during the carbonization process of the precursor and the incomplete fill by carbon, the pore diameter of CMK-3 is lower than the pore wall thickness of SBA-15 (4.39 nm). CMK-3 exhibits large surface areas and pore volume, as shown in Table 1; the S_{BET} and pore volume of CMK-3 reach 1,480 $m^2 g^{-1}$ and 1.59 $cm^3 g^{-1}$, respectively.

2. Surface Elemental Composition and Functional Groups

XPS and FT-IR spectra were employed to determine the surface elemental composition and function groups of CMK-3. XPS survey spectrum, as is shown in Fig. 2(a), indicate that the surface components of CMK-3 are mainly carbon and oxygen. Meanwhile, the O content on surface reaches 5.76 at%, indicating that an abundance of oxygen groups is present on the surface of CMK-3. A closer look at the XPS spectrum of the C1s orbital (Fig. 2(b)) shows several relatively well-resolved peaks corresponding to carbon atoms in different chemical environments. The most dominant contribution around 284.5 eV comes from aromatic or other sp^2-hybridized carbon atoms bound to neighboring carbon atoms or hydrogen. Fur-

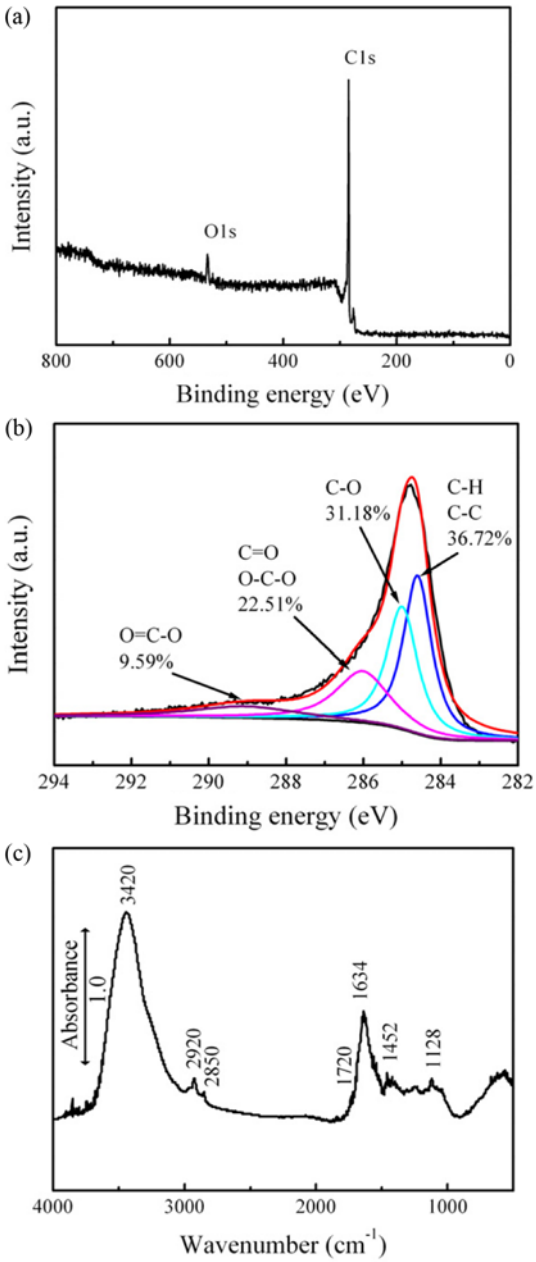

Fig. 2. XPS spectra of CMK-3 (a); high-resolution XPS C1s spectra of CMK-3 (b); FT-IR spectrum of CMK-3 (c).

thermore, hydroxy/ether groups (C-O, B.E.=285.5 eV), carbonyl groups (C=O, B.E.=286.2 eV) and carboxyl groups (COOH, B.E.= 288.9 eV) can be identified [17-19]. The oxygen groups were further attested by the FT-IR spectrum. As shown in Fig. 2(c), the presence of oxygen groups is evidenced by the bands at 3,000-3,700 cm^{-1} (a wide band attributed to OH stretching vibrations in hydroxyl or carboxyl groups), 1,720 cm^{-1} (C=O vibrations corresponding to carbonyl, quinone, ester, or carboxyl) and 1,000-1,300 cm^{-1} (C-O stretching vibrations in hydroxy, ester, or ether and OH bending vibrations) [20]. Moreover, the presence of aliphatic structures is suggested by the band at 2,920 and 2,850 cm^{-1}, which corresponds to stretching vibrations of aliphatic chains (-CH) [21]. The presence of hydroxy groups and aliphatic structure illustrates that carbonization of sucrose by sulfuric acid is incomplete, a great number of sucrose molecule fragments with numerous oxygen groups are still present on the surface of CMK-3.

3. Electrochemical Performance of CMK-3 in Calcium Nitrate Aqueous Electrolyte

Cyclic voltammetry is suitable for estimating the difference between the non-Faradaic and Faradaic reactions and can also be used for preliminary determination of the power density and energy density of supercapacitors [22]. Fig. 3 presents the cyclic voltammograms (CVs) of CMK-3 in different aqueous electrolytes at a rate of 10 mV/s. As shown in Fig. 3, the CMK-3 electrode exhibits a wide voltage window from −1.0 to 0.8 V in $Ca(NO_3)_2$ and $NaNO_3$ aqueous solution, which is higher than conventional KOH aqueous electrolyte. This is very vital in the enhancement in energy density (E) as E is proportional to the squared of V according to $E=1/2\ CV^2$ [1]. Moreover, the CV curves of the CMK-3 electrode in KOH aqueous electrolyte exhibit an approximately rectangular shape without obvious redox peaks, indicating typical double-layer capacitance behavior. Nevertheless, the CV curves in $Ca(NO_3)_2$ and $NaNO_3$ aqueous electrolyte both deviate from idealized double-layer behavior with a pair of broad, superimposed and reversible faradaic surface redox reactions (an oxidation peak at about −0.3 V, and a reduction oxidation peak at about −0.5 V), behaving as pseudo-capacitance. That may be due to the surface oxygen groups on the surface of CMK-3 which induce the complex faradic reactions in $Ca(NO_3)_2$ and $NaNO_3$ aqueous solution, and thus enhance the pseudo-capacitance. It is clear that the CMK-3 electrode exhibits larger CV areas in $Ca(NO_3)_2$ aqueous electrolyte than that in KOH and $NaNO_3$ aqueous electrolytes, suggesting higher specific capacitances in $Ca(NO_3)_2$ aqueous electrolyte compared with that in KOH and $NaNO_3$ aqueous electrolyte, respectively. This may be because the specific capacitance of CMK-3 electrode in $Ca(NO_3)_2$ aqueous electrolyte is contributed by pseudo-capacitance as well as double-layer capacitance, and the divalent Ca^+ cation possesses more charges than univalent K^+ or Na^+ cation, which allows CMK-3 electrode to store more energy on per unit surface area (as shown in Table 2).

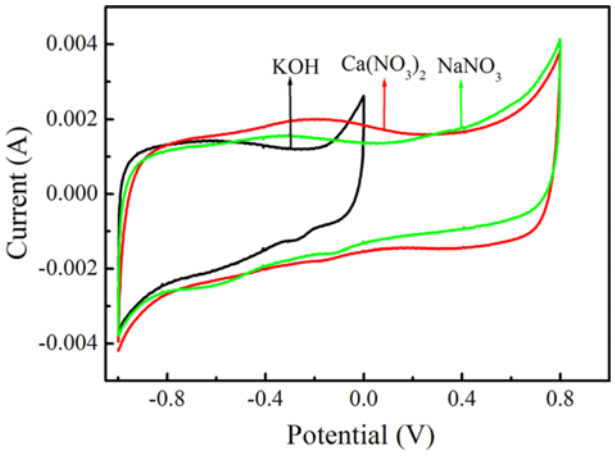

Fig. 3. CV curves of CMK-3 electrode in different aqueous electrolytes at a rate of of 10 mV/s.

Table 2. The specific gravimetric capacitances (C_g) and specific capacitances per surface area (C_{SA}) of CMK-3 electrode in different aqueous electrolyte

Electrolyte	C_g (F g^{-1})					C_{SA}[a] (F m^{-2})
	1 A g^{-1}	2 A g^{-1}	5 A g^{-1}	10 A g^{-1}	20 A g^{-1}	
$Ca(NO_3)_2$	210	179	145	126	111	0.14
$NaNO_3$	150	145	123	119	110	0.10
KOH	136	120	107	100	95	0.09

[a] $C_{SA}=C_{g\,(1\ A/g)}/S_{BET}$

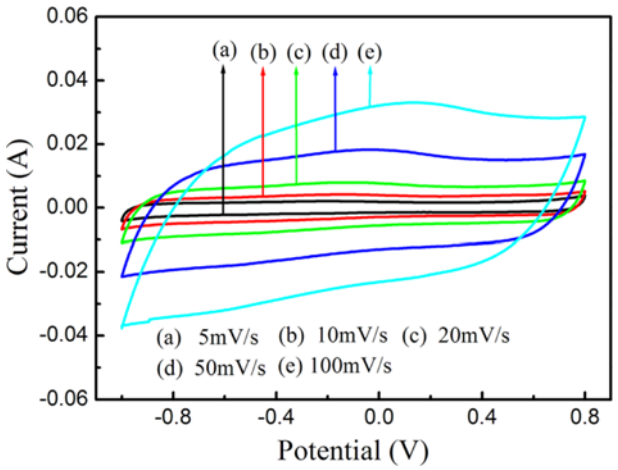

Fig. 4. CV curves of of CMK-3 electrode in $Ca(NO_3)_2$ aqueous electrolyte at various scan rates.

Fig. 4 shows the CV curves of CMK-3 electrode in $Ca(NO_3)_2$ aqueous electrolyte at various scan rates from 5 to 100 mV/s. As shown in Fig. 4, the CV curves exhibit a stable shape over a wide rate range (5-50 mV/s) with proportional increase of the peak area. The obvious increase of peak area with scan rate and the rapid current response on voltage reversal at each end potential indicate a good kinetic process of Ca^{2+} diffusion in the pores of CMK-3 electrode. Also, these features indicate that CMK-3 electrode is stable at both low and high scan rates in $Ca(NO_3)_2$ aqueous electrolyte, especially under the situation in which remarkably accelerated charge propagation in the pores of the electrode is involved.

The pseudo-capacitance may originate from the redox reactions between -COOH and -CO functional groups on the surface of CMK-3 in $Ca(NO_3)_2$ aqueous electrolyte. The possible redox mechanism is shown in Fig. 5. The carboxyl groups have great adsorption capacity for Ca^{2+}, which can replace the H^+ of the -COOH functional groups, and form $-COOCa^+$. The empty valence orbit of the calcium atoms

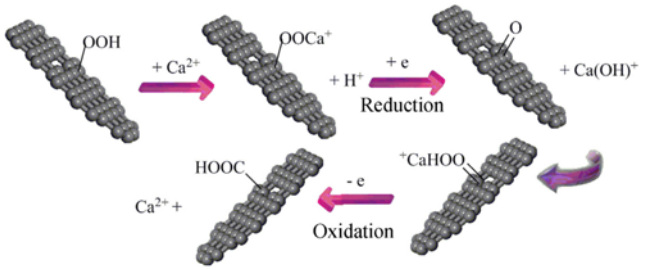

Fig. 5. The possible redox reactions on the surface of CMK-3 electrodes in $Ca(NO_3)_2$ aqueous electrolyte.

has a strong affinity for the lone pair electrons on the 2p orbit of oxygen, which weakens the bond energy of C-O bond, and is favorable for the reduction of -COOH groups to -CO groups. In the reduction process, a -$COOCa^+$ group gets one electron from the electrode, and deoxidizes to an aldehyde group. In the oxidation process, aldehyde groups attract $Ca(OH)^+$ to form -$COOHCa^+$, and oxidate to carboxyl groups by loss of one electron and release the Ca^{2+} ions. Compared with the Ca^{2+} ion, K^+ and Na^+ ions have a weak effect with the -COOH groups, CMK-3 carbon electrode, thus exhibiting the unapparent pseudo-capacitance in KOH and $NaNO_3$ aqueous electrolytes.

The electrochemical impedance behavior of CMK-3 electrode in different aqueous electrolytes is shown in Fig. 6. The Nyquist plots of the CMK-3 electrode in all aqueous electrolytes exhibit the typical features of porous electrodes with a 45° Warburg region at high-medium frequencies and an almost vertical line at low frequencies, where the behavior becomes mainly capacitive [23]. Moreover, the Nyquist plot of CMK-3 electrode shows a semicircle in the high frequency region in all aqueous electrolytes, which is caused by the charge transfer resistance representing an electrochemistry controlled process at the interface between electrode and electrolyte [24]. The diameter of the semicircle in $Ca(NO_3)_2$ electrolyte is smaller than that in $NaNO_3$ electrolyte, revealing the reduced charge transfer resistance of CMK-3 electrode in $Ca(NO_3)_2$ electrolyte due to the more charges of divalent Ca^{2+} ion than univalent Na^+. Furthermore, in the high frequency region, the intercept at the real impedance (Z′) axis is related to the internal resistance, including the ionic resistance of the electrolyte, intrinsic resistance of CMK-3 electrode and their contact resistance with Ni foam current collector [23,24]. CMK-3 electrode exhibits larger ionic resistance in $Ca(NO_3)_2$ electrolyte, as shown in Fig. 6, the internal resistance of CMK-3 electrode in $Ca(NO_3)_2$ electrolyte is 1.72 Ω, which is obviously larger than that in KOH (1.15 Ω) and $NaNO_3$ (1.09 Ω) electrolytes. This may be because the diameter of hydrated Ca^{2+} ion in aqueous solution is larger than that of hydrated K^+ and Na^+ ion and higher ionic resistance of the electrolyte.

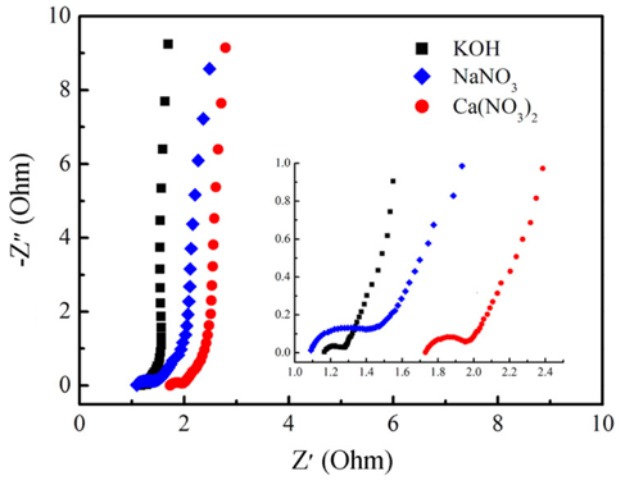

Fig. 6. Nyquist impedance plots of CMK-3 electrode in different aqueous electrolytes.

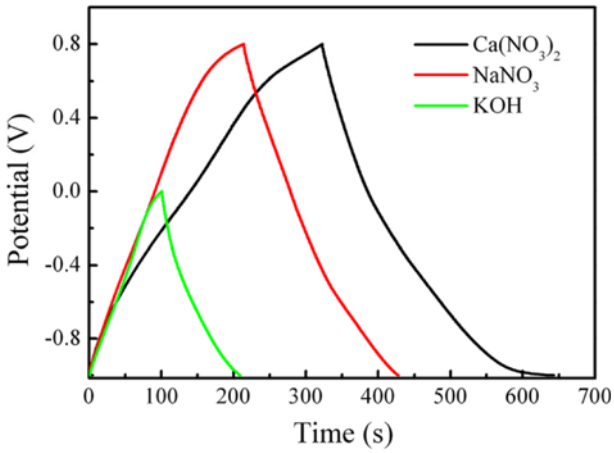

Fig. 7. The galvanostatic charge-discharge curves of CMK-3 electrode in different aqueous electrolytes at a current density of 1 A g^{-1}.

Fig. 7 shows the galvanostatic charge-discharge curves of CMK-3 electrode measured at a current density of 1 A g^{-1} in different aqueous electrolytes. The nearly triangular charge and discharge curves reflect the good capacitive performance of CMK-3 electrode in the investigated aqueous electrolytes. The specific gravimetric capacitance C (F g^{-1}) calculated from the discharge curve under different current densities is summarized in Table 2. CMK-3 electrode exhibits more superior specific capacitance in $Ca(NO_3)_2$ electrolyte, which specific gravimetric capacitance reaches 210 F g^{-1} while that in $NaNO_3$ and KOH electrolytes is 150 and 136 F g^{-1}. The specific gravimetric capacitance in $Ca(NO_3)_2$ electrolyte is higher than that in $NaNO_3$ and KOH electrolytes, about 40% and 54%, respectively. Moreover, the specific capacitance per surface area C_{S4} of CMK-3 electrode in $Ca(NO_3)_2$ electrolyte at current density of 1 A g^{-1} reaches 0.14 F m^{-2}, which is higher than that in $NaNO_3$ (0.10 F m^{-2}) and KOH (0.09 F m^{-2}) electrolytes. The reason for the high specific gravimetric capacitance in $Ca(NO_3)_2$ electrolyte may be that: 1) divalent Ca^{2+} ion possesses more charge than univalent K^+ and Na^+ ion, which is favorable for the electrostatic attraction between the electrode and electrolyte and results in the higher charge density of the electric double layer formed at the interface of the CMK-3 electrode and $Ca(NO_3)_2$ electrolyte, and then allows CMK-3 electrode to store more energy on per surface area. 2) The pseudo-capacitive effect originating from the oxygen groups on the surface of CMK-3 in $Ca(NO_3)_2$ electrolyte contributes additional capacitance. Fig. 7 gives the galvanostatic charge/discharge curves of CMK-3 electrode in $Ca(NO_3)_2$ electrolyte at different loading current density. As shown in Fig. 8 and Table 2, the specific capacitance of CMK-3 electrode in $Ca(NO_3)_2$ is about

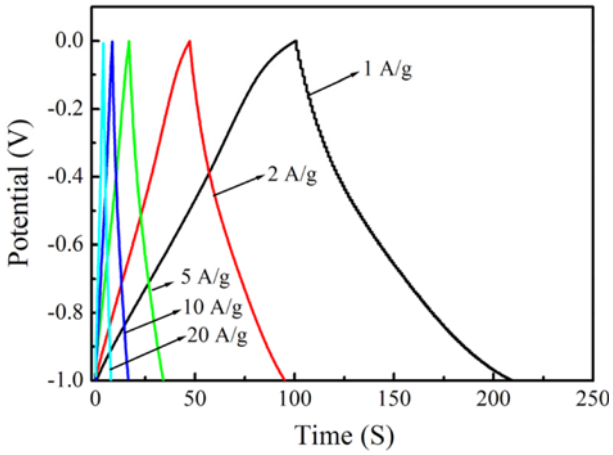

Fig. 8. The galvanostatic charge/discharge curves of CMK-3 electrode in $Ca(NO_3)_2$ electrolyte at different loading current density.

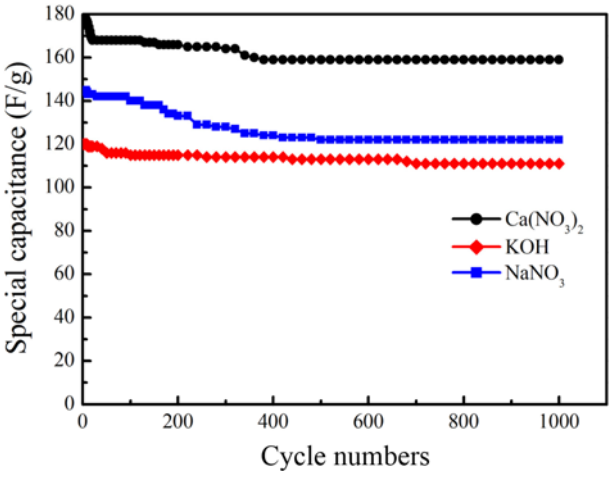

Fig. 9. The cycle performance of CMK-3 electrodes in $Ca(NO_3)_2$ electrolyte.

111 F g^{-1} at a high current density of 20.0 A g^{-1} with the retention of 52.8%, which indicates the unsatisfactory rate capability. In despite of that, the specific capacitance in $Ca(NO_3)_2$ electrolyte is still higher than that in $NaNO_3$ and KOH electrolytes at the same current density. These results demonstrate that $Ca(NO_3)_2$ solution can be used as an excellent aqueous electrolyte for supercapacitors. It should be noted that the capacitance retention of CMK-3 electrode in $Ca(NO_3)_2$ electrolyte after 1000 cycles at a current density of 2 A g^{-1} is as high as ~92.6%, which is very close to that in KOH electrolytes (92.4%), as shown in Fig. 9, confirming the excellent electrochemical stability.

CONCLUSIONS

Due to the high charge density of the electric double layer formed at the interface of the CMK-3 electrode and $Ca(NO_3)_2$ aqueous electrolyte and the pseudo-capacitive effect originating from the oxygen groups on the surface of CMK-3 in $Ca(NO_3)_2$ aqueous electrolyte, mesoporous carbon CMK-3 exhibits excellent electrochemical properties with wide voltage window, high specific gravimetric capacitance and satisfactory electrochemical stability in $Ca(NO_3)_2$ aqueous electrolyte. The specific gravimetric capacitance of CMK-3 electrode in $Ca(NO_3)_2$ aqueous electrolyte reaches 210 F g^{-1} at a current density of 1 A g^{-1}, which is higher than that in $NaNO_3$ and KOH electrolytes about 40% and 54%, respectively. The capacitance retention of CMK-3 electrode in $Ca(NO_3)_2$ aqueous electrolyte after 1000 cycles at a current density of 2 A g^{-1} is as high as ~92.6%. These results demonstrate that $Ca(NO_3)_2$ aqueous solution can be used as a satisfactory aqueous electrolyte for supercapacitors.

ACKNOWLEDGEMENTS

This work was supported by the National Natural Science Foundation of China under Grant No. 51063003; the Natural Science Foundation of Gansu under Grant No. 1112RJZA024; State Key Laboratory of Gansu Advanced Non-ferrous Metal Materials under Grant No. SKL1311; the Key Laboratory of Eco-Environment-Related Polymer Materials of the Ministry of Education Program under Grant No. KF-13-01, and the Hongliu young teacher cultivate project of Lanzhou University of Technology under Grant No. Q201112.

REFERENCES

1. Y. Zhai, Y. Dou, D. Zhao, P. F. Fulvio, R. T. Mayes and S. Dai, *Adv. Mater.*, **23**, 4828 (2011).
2. W. Xiong, M. Liu, L. Gan, Y. Lv, Y. Li, L. Yang, Z. Xu, Z. Hao, H. Liu and L. Chen, *J. Power Sources*, **196**, 10461 (2011).
3. X. Zhao, Q. Zhang, C.-M. Chen, B. Zhang, S. Reiche, A. Wang, T. Zhang, R. Schlögl and D. Sheng Su, *Nano Energy*, **1**, 624 (2012).
4. Y. Lv, F. Zhang, Y. Dou, Y. Zhai, J. Wang, H. Liu, Y. Xia, B. Tu and D. Zhao, *J. Mater. Chem.*, **22**, 93 (2012).
5. D. Hulicova, M. Kodama and H. Hatori, *Chem. Mater.*, **18**, 2318 (2006).
6. K. Y. Kang, S. J. Hong, B. I. Lee and J. S. Lee, *Electrochem. Commun.*, **10**, 1105 (2008).
7. J.-w. Lang, X.-b. Yan, W.-w. Liu, R.-t. Wang and Q.-j. Xue, *J. Power Sources*, **204**, 220 (2012).
8. Z. Lei, D. Bai and X. S. Zhao, *Micropor. Mesopor. Mater.*, **147**, 86 (2012).
9. D. A. Links, *J. Mater. Chem.*, **22**, 24213 (2012).
10. Y. S. Yun, J. Shim and H.-j. Jin, *RSC Advances*, 4353 (2012).
11. C.-C. Hu, W.-Y. Li and J.-Y. Lin, *J. Power Sources*, **137**, 152 (2004).
12. Y. Munaiah, B. G. Sundara Raj, T. Prem Kumar and P. Ragupathy, *J. Mater. Chem. A*, **1**, 4300 (2013).
13. K.-S. Kim and S.-J. Park, *Micropor. Mesopor. Mater.*, **163**, 140 (2012).
14. D. Zhao, J. Feng, Q. Huo, N. Melosh, G. H. Fredrickson and B. F. Chmelka, *Science*, **279**, 548 (1998).
15. S. Jun, S. H. Joo, R. Ryoo and M. Kruk, *J. Am. Chem. Soc.*, **122**, 10712 (2000).
16. Y. Xia and R. Mokaya, *Adv. Mater.*, **16**, 1553 (2004).
17. R. Liu, D. Wu, X. Feng and K. Müllen, *Angew. Chem. Int. Ed.*, **49**, 2565 (2010).
18. G. P. Mane, S. N. Talapaneni, C. Anand and S. Varghese, *Adv. Funct. Mater.*, **22**, 3596 (2012).
19. D.-Y. Zhang, Y. Ma, H. Feng, Y. Wang and Y. Hao, *Adv. Powder Technol.*, **23**, 215 (2011).
20. Y. Zhai, Y. Dou, X. Liu, B. Tu and D. Zhao, *J. Mater. Chem.*, **19**,

3292 (2009).
21. Z. Wu, P. A. Webley and D. Zhao, *J. Mater. Chem.*, **22**, 11379 (2012).
22. H.-L. Jiang, B. Liu, Y.-Q. Lan, K. Kuratani, T. Akita, H. Shioyama, F. Zong and Q. Xu, *J. Am. Chem. Soc.*, **133**, 11854 (2011).
23. J. Zhou, X. Yuan, W. Xing, W. Si and S. Zhuo, *Carbon*, **48**, 2765 (2010).
24. D. S. Dhawale, M. R. Benzigar, M. a. Wahab, C. Anand, S. Varghese, V. V. Balasubramanian, S. S. Aldeyab, K. Ariga and A. Vinu, *Electrochim. Acta*, **77**, 256 (2012).